surfaces

MDPI

Article

Applicability of Fluorine Gas Surface Treatment to Control Liquid Sodium Wettability

Masanari Namie [1,*], Jun-ichi Saito [1], Asuka Ikeda [1], Ryotaro Oka [2] and Jae-Ho Kim [2]

[1] Tsuruga Comprehensive Research and Development Center, Japan Atomic Energy Agency, Tsuruga 919-1279, Japan; saito.junichi78@jaea.go.jp (J.-i.S.); ikeda.asuka@jaea.go.jp (A.I.)
[2] Department of Materials Science and Engineering, Faculty of Engineering, University of Fukui, 3-9-1 Bunkyo, Fukui 910-8507, Japan; mi230306@g.u-fukui.ac.jp (R.O.); kim@matse.u-fukui.ac.jp (J.-H.K.)
* Correspondence: namie.masanari@jaea.go.jp

Abstract: The iron (Fe) specimens selected as the substrate metal for this study were surface-treated using fluorine gas, and their wettability with liquid sodium (Na) was evaluated using the sliding angle. Additionally, the surface morphology and binding state were analyzed, and the applicability of wettability control with liquid sodium by fluorination was discussed using the analysis results. Fluorination formed a fluoride layer comprising FeF_2 and FeF_3 bonds on the iron surface. The composition of the fluoride layer varied, depending on the treatment conditions. The surface of the specimen that contains a lot of FeF_3 bonds had a small sliding angle for the liquid sodium droplet and was harder to wet than the untreated specimen. In contrast, the surface of the specimen that contains a lot of FeF_2 bonds had a large sliding angle for the liquid sodium droplet and was easier to wet than the untreated specimen. These results indicate that fluorination is an effective surface modification technique that can be applied to control the wettability of iron with liquid sodium.

Keywords: wettability; surface treatment; iron fluoride; liquid sodium; interface

Citation: Namie, M.; Saito, J.-i.; Ikeda, A.; Oka, R.; Kim, J.-H. Applicability of Fluorine Gas Surface Treatment to Control Liquid Sodium Wettability. *Surfaces* **2024**, *7*, 550–559. https://doi.org/10.3390/surfaces7030037

Academic Editor: Gaetano Granozzi

Received: 23 May 2024
Revised: 6 August 2024
Accepted: 7 August 2024
Published: 9 August 2024

1. Introduction

Liquid sodium (liquid Na) is used as a coolant in fast breeder reactors because it does not slow down fast neutrons, has high thermal conductivity, and has a wide temperature range as a liquid [1–4]. Liquid Na contacts a diverse range of equipment in fast reactors; therefore, its wettability affects the performance of these pieces of equipment.

For example, liquid metal embrittlement (LME) of structural materials due to liquid Na results from liquid Na penetrating into the grain boundaries of the material; therefore, wettability with the material is crucial [5,6]. If the wettability between the structural material and liquid Na is poor, liquid Na will not penetrate, and LME will not occur. Wettability with liquid metal is important for heat transfer capacity in heat exchangers [7]. If the wettability between the heat transfer tube and liquid Na is good, heat is transferred efficiently. Furthermore, the wettability of the sensor surface with liquid Na is essential for the high sensitivity of the ultrasonic flowmeter to transmit and receive ultrasonic waves [8–11]. If the wettability between the transmitting and receiving surfaces and liquid Na is good, the transmitting and receiving performance will be improved.

Thus, the wettability requirements differ depending on the application of the equipment. Some studies have investigated the wetting behavior of liquid Na for various temperatures and metals to control wettability and meet these requirements [12–15].

However, mechanical and thermal properties are more significant in actual equipment design than wettability, and materials with excellent properties in these areas are used. Therefore, materials possessing wettability with liquid Na suitable for the equipment are not necessarily used. Controlling the wettability of structural materials in contact with liquid Na can improve the operating efficiency and safety of fast reactors. Consequently, a

surface treatment was investigated that did not change the fundamental properties of the structural material but only the wettability of the surface to meet the required properties.

In this study, iron (Fe), the primary composition of stainless steel, was surface-treated with fluorine gas (F_2) to investigate its wettability with liquid Na. F_2 is a straightforward molecule of fluorine—a gas with high reactivity. In addition, fluorine has various specificities, such as possessing the highest electronegativity and relatively stable fluoride bonds formed after fluorination [16,17]. Surface fluorination, using the specificity and reactivity of F_2, can control the surface morphology and binding state of organic and metallic materials [18–23].

In previous studies, we reported that the electronic state and the atomic interactions at the interface could affect wettability [24]. Therefore, we presume that fluorination changes the wettability of structural materials with liquid Na. This study aims to develop wettability control technology for structural materials with liquid Na by surface fluorination. This study reports the surface morphology analysis results of fluorinated iron surfaces and an evaluation of liquid Na wettability. First, the iron surface is fluorinated. The surface state of the specimens was observed using techniques such as X-ray photoelectron spectroscopy and scanning electron microscopy to discuss the reaction between the iron and F_2 gas and the products. Next, the wettability of the fluorinated specimens with liquid Na was evaluated. Finally, from the relationship between the surface state formed by fluorination and the wettability with liquid Na, we examined the applicability of fluorination on the control of liquid Na wettability.

2. Experiments

2.1. Surface Fluorination

An iron (Fe) plate manufactured by The Nilaco Corporation (FE-223383, 99.5%) was used as the substrate. The test specimens (40 × 40 mm) were cut from iron plates for analysis and wettability experiments and ultrasonically cleaned in acetone. The test specimens were sealed in a nickel reactor and connected to a fluorination apparatus described in a previous paper by the authors [25]. The fluoridation conditions were based on those used in our previous study [22]. The F_2 gas pressures in the reactor were 380 Torr (50.7 kPa) or 760 Torr (101.3 kPa), the reaction temperatures were room temperature (25 °C), 100 °C, or 200 °C, and a reaction time of 24 h was used for fluorination conditions. Table 1 shows the fluorination conditions. The specimen names in Table 1 indicate the gas pressure and reaction temperature used in fluorination. Untreated indicates unfluorinated specimens.

Table 1. Specimen names and fluorination conditions.

Specimen Names	Material	Fluorination Conditions		
		Fluorine Gas Pressure /Torr (kPa)	Temp. /°C	Time /hour
Untreated	Fe	—	—	—
F-380-RT		380 (50.7)	RT (25)	24
F-760-RT		760 (101.3)	RT (25)	24
F-380-100		380 (50.7)	100	24
F-380-200		760 (101.3)	100	24
F-760-100		380 (50.7)	200	24
F-760-200		760 (101.3)	200	24

2.2. Surface Morphology Analysis

The untreated and fluorinated specimens were measured for surface morphology and binding state. The surface morphology was observed for secondary electron images using field emission scanning electron microscopy (SEM; ZEISS Gemini SEM, Carl Zeiss, Stuttgart, BW, Germany). The surface roughness was also measured using atomic force microscopy (AFM; Nanoscope IIIa, Digital Instruments, Inc., Tonawanda, NY, USA). The

AFM measurements were performed in contact mode, measuring an area of 10 µm square. The binding energy was measured using an X-ray photoelectron spectrometer (JPS-9010, JOEL, Tokyo, Japan). Mg Kα (λ = 1253.6 eV) was the X-ray source. The obtained X-ray photoelectron spectroscopy (XPS) spectra were corrected for charge shift by aligning the carbon impurity peak to 284.0 eV.

2.3. Liquid Na Wettability Test

The sliding method was used for the wettability test in this study. The specimen was placed on a ceramic hot plate placed horizontally on a tiltable table, and 500 µL of Na droplet was added dropwise onto it. The temperature of the specimen and the Na droplet was 150 °C. After 3 min of adding the Na droplet onto the specimen, the tiltable table was tilted at 1°/s until the droplet slid down. The angle at which the droplet slid down was recorded as the sliding angle. Advancing and receding contact angles were measured from the shape of the droplet as it slid down using a video taken with a camera. (Figure 1) The measurements were performed five or more times for each specimen, and the average value was taken as the evaluation value.

Liquid Na is highly reactive, and its surface oxidizes rapidly when it makes contact with oxygen or water vapor in the air. Therefore, we performed the wettability test for the specimen using liquid Na in a glove box filled with high-purity argon gas to prevent the surface oxidation of the Na droplets. The oxygen concentration in the glove box is less than 3 ppm, and the dew point is less than −69 °C.

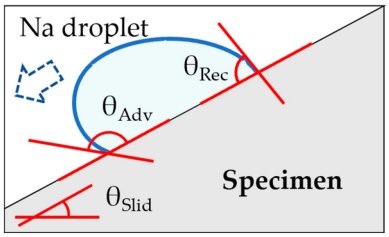

Figure 1. Schematic diagram of wettability parameters obtained by wettability testing.

3. Results

3.1. Surface Binding State

Figure 2 shows the Fe 2p3/2 peaks on the outermost surface of the specimens measured using XPS. Two peaks near 710 and 714 eV were observed on the surface of the fluorinated specimens. Kasrai et al. reported that the FeF_2 and FeF_3 peaks, typical iron fluorides, were detected at 710.2 and 714.2 eV, respectively [26]. Therefore, in Figure 2, the peak detected on the high-energy side should be FeF_3 bonds, and the peak detected on the low-energy side should be FeF_2 bonds.

Figure 3 shows the fitting results of the Fe 2p3/2 peaks for F-380-RT and F-760-200. Since only FeF_2 and FeF_3 peaks are used for fitting, nonstoichiometric compounds resulting in FeF_x ($x < 2$, $2 < x < 3$) are not considered. In F-380-RT, the ratio of each iron fluoride peak was FeF_2:FeF_3 = 11.6:88.4, and the bonding of the outermost surface was FeF_3 bonding-rich. In F-380-200, the peak ratio of each iron fluoride was FeF_2:FeF_3 = 72.6:27.4, and the bonding of the outermost surface was FeF_2 bonding-rich. From the above, the FeF_3 bonding-rich surface or FeF_2 bonding-rich surface was formed on the specimen by adjusting the fluorination conditions. However, only the FeF_2 or FeF_3 bond was not formed on the specimen surface. Furthermore, since this is a surface treatment method involving F_2 gas contact, the bond of the nonstoichiometric compound FeF_x ($x < 2$, $2 < x < 3$) might exist on the specimen surface. Therefore, the specimen surface formed by fluorination was thought to have a complex bonding state.

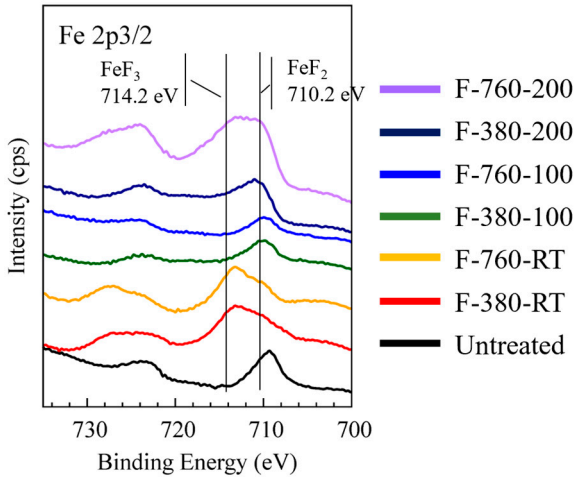

Figure 2. XPS spectra (Fe 2p3/2) of untreated and fluorinated specimens.

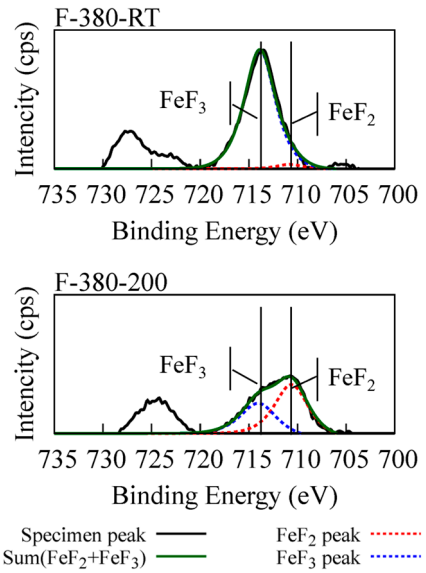

Figure 3. Fitting results of the Fe 2p3/2 peaks for F-380-RT and F-380-200 specimens.

Figure 4 shows the measurement results of the Fe 2p3/2 peak when the surface of the F-760-100 and F-380-RT specimens was etched to a depth of 20 nm using argon ion. The etching changed the binding state on the surface of the F-760-100 specimen, where the metal Fe peak appeared and became stronger, and the fluoride peak became significantly weaker. In contrast, iron peak was not detected in the F-380-RT specimen even after etching to 20 nm, and only fluoride peaks were detected. It was suggested that the fluoride layer on the F-760-100 specimen was thinner than that on the F-380-RT specimen. As a result of depth analysis using XPS, F-380-RT, F-760-RT, and F-760-200 formed a thick fluoride layer, and F-380-100, F-760-100, and F-380-200 formed a thin fluoride layer. For example, the thickness of the fluoride layer of F-760-100 was about 20 nm or less, and the thickness of the fluoride layer of F-760-200 was 250 nm or more.

3.2. Surface Morphology

Figure 5 shows the surface morphology of various untreated and fluorinated specimens. Ra in the figure indicates the arithmetic mean roughness. The surface roughness of the F-380-RT, F-760-RT, and F-760-200 specimens was approximately 3–6.5 times larger than that of the untreated specimens, resulting in a very coarse surface. In contrast, the

surface roughness of the specimens fluorinated at 100 °C (F-380-100, F-760-100) was similar to that of the untreated specimens.

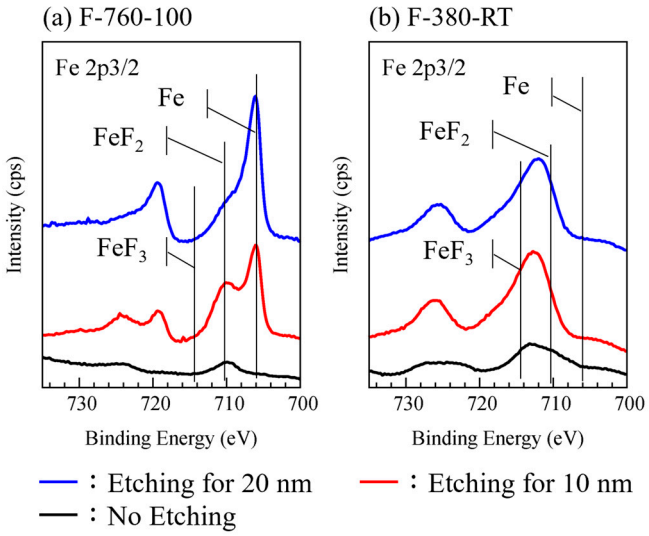

Figure 4. Changes in the surface binding state of specimens by argon ion etching.

Figure 6 shows the surface morphology of the F-380-RT specimen using SEM analysis. This figure shows the lower magnification image of F-380-RT than the image of Figure 5. The fluoride layer was created on the surface of the specimens by fluorinating even at room temperature (25 °C); they have coarse surfaces and many cracks.

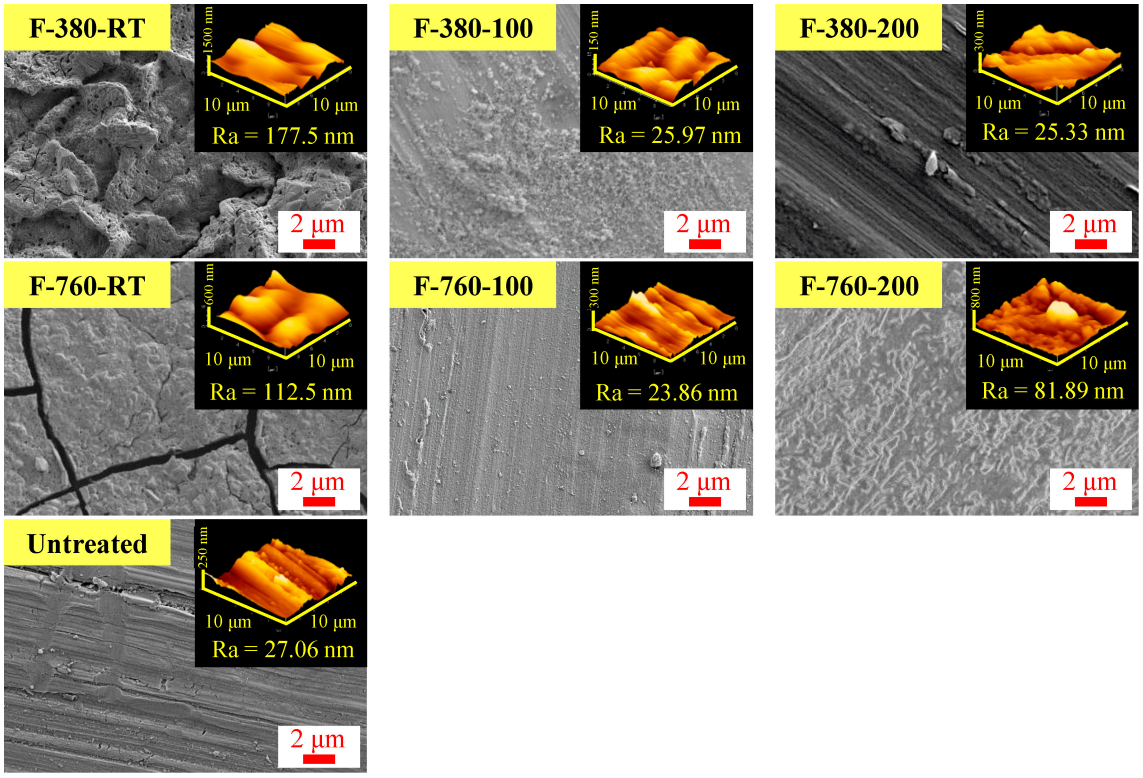

Figure 5. Surface morphology and roughness of each specimen.

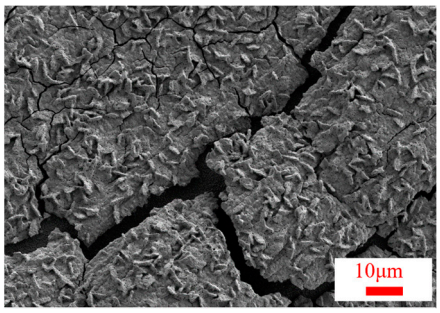

Figure 6. Low magnification SEM image of F-380-RT specimen.

3.3. Liquid Na Wettability

Figure 7 shows the sliding angles of Na droplets for various specimens. Compared to the sliding angle of the untreated specimen, those of F-380-RT, F-760-RT, and F-760-200 were extremely small. In contrast, the sliding angles of F-380-100, F-760-100, and F-380-100 were larger than those of the untreated specimen. Among the sliding angle measurement results of each substrate obtained, Untreated, F-760-100, and F-380-RT were compared with a t-test between two groups and multiple comparison methods to confirm the effect of the fluorination. F-760-100 and F-380-RT are the closest specimens to Untreated among the groups that have changed to the smaller side (or larger side) of the sliding angle. A significant difference was obtained between Untreated and F-380-RT ($t(8) = 2.31$, $p < 0.001$, $T = 18.43$), and there was also a significant difference between Untreated and F-760-100 ($t(7) = 2.36$, $p < 0.001$, $T = 6.70$). It was shown that the liquid sodium wettability of iron was significantly changed by fluorination treatment.

The above clarifies the effect of fluorination on the wettability of liquid Na. Furthermore, depending on the fluorination conditions, the wettability of liquid Na changed to lyophilic and lyophobic states. Figure 8 shows the advancing and receding contact angles when a Na droplet slides down the specimen surface. Compared with the untreated specimen, the receding contact angles of F-380-RT, F-760-RT, and F-760-200 are larger, whereas those of F-380-100, F-760-100, and F-380-200 are smaller. The difference between each specimen was smaller in the advancing contact angle than in the receding contact angle.

Figure 9 shows the shape of the Na droplet as it slides down the specimen surface. The shape deformation of the Na droplet was small when it slid down the F-760-200 specimen in Figure 9b. In contrast, the shape deformation of the Na droplet was large when it slid down the F-380-200 specimen in Figure 9c.

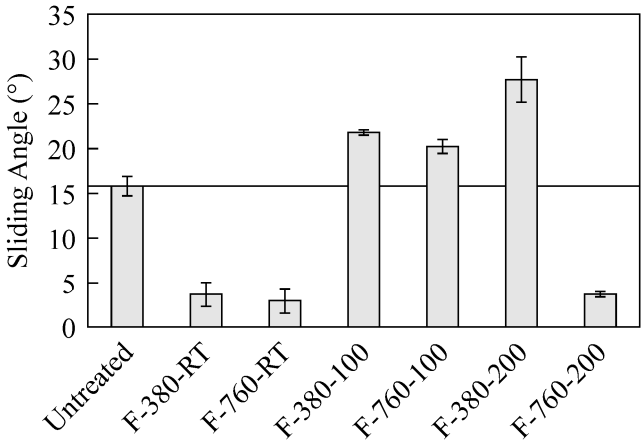

Figure 7. Sliding angles of Na droplets for various specimens.

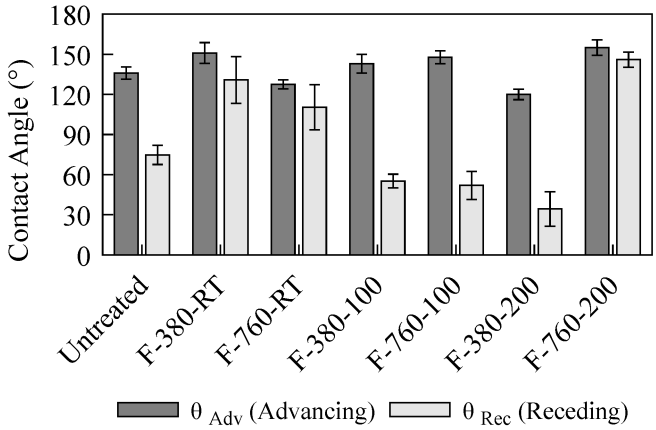

Figure 8. Advancing and receding contact angles of each specimen.

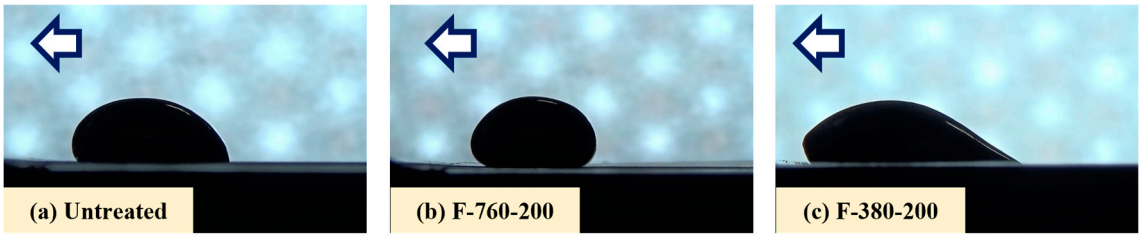

Figure 9. Shape of liquid Na droplets during sliding (the arrow is the sliding direction of the droplet).

4. Discussions

4.1. Formation Process of Fluoride Layer by Surface Fluorination

The surface analyses revealed two fluoride layers with different major bonds and thicknesses. The reaction temperature in the fluorination process has a greater effect on the modification layer characteristics than the gas pressure. Here, we discuss the formation of two types of fluoride layers that significantly affect liquid Na wettability.

One is the formation process of the specimens fluorinated at room temperature and with thick fluoride layers. Figure 10 shows a schematic diagram of its fluoride layer cross-section. As shown in Figure 6, a noticeable fluoride layer was produced on the surface of the F-380-RT specimen that was fluorinated at room temperature. Furthermore, Figure 4 shows that the fluoride thickness of F-380-RT was thicker than that of F-760-100. A strong peak of the FeF_3 bond was detected by XPS (Figure 3). Therefore, it can be inferred that a fluoride layer is formed on the specimen's surface by being fluorinated at room temperature. Many cracks appear in the fluoride layer, which might result from thermal stresses due to temperature differences within the fluoride layer. Additionally, although there are few studies on surface modification of iron by direct fluorination, it has been reported that fluorination of stainless steel, which is mainly composed of iron, may cause cracks in the fluoride layer formed according to fluorination conditions [20]. It is assumed that the F_2 migrated to the iron surface through cracks in the fluoride layer or by diffusion phenomena within the fluoride layer. Therefore, the upper part of the fluoride layer appears to have a higher fluorine concentration, whereas the lower part has a lower concentration. The analysis results and speculations indicate that layers at the surface of the specimen fluorinated at room temperature comprise two types. One is a reaction layer ($FeF_{(1–3)}$-like) where F_2 gas and iron react. The other is a growing layer (FeF_3-like) where the reaction produces the fluoride.

The other formation process involves the specimens fluorinated at high temperatures and with thin fluoride layers. Figure 11 shows a schematic diagram of its fluoride layer cross-section. A strong peak of the FeF_2 bond was detected on the surface of the F-760-100 specimen fluorinated at 100 °C by XPS analysis, and its fluoride layer was thin (Figure 4).

Therefore, as shown in Figure 11, the specimen surface fluorinated with heat has a fluoride layer (FeF_3) that is quickly formed and peeled due to thermal stress frequently occurring, and a reaction layer primarily comprising FeF_2 bonds might be exposed on the surface. This process would be applied to the specimens fluorinated at high temperatures but not to F-760-200, which was fluorinated with heat, but that surface condition was close to a specimen fluorinated at room temperature. From the comparison with F-380-200, the F_2 gas pressure might cause the difference but a further experimental investigation is required to explain it.

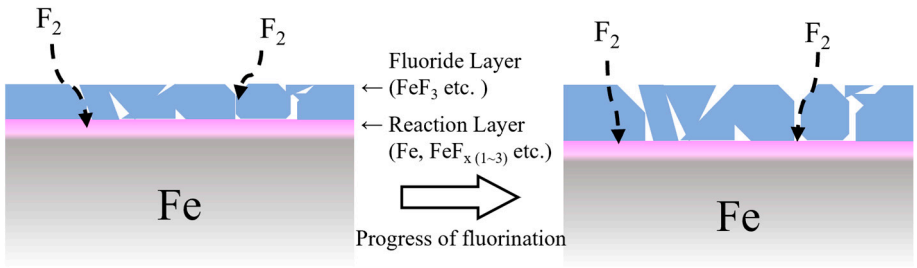

Figure 10. Schematic diagram of the fluoride layer cross-section formed on the surface by fluorination.

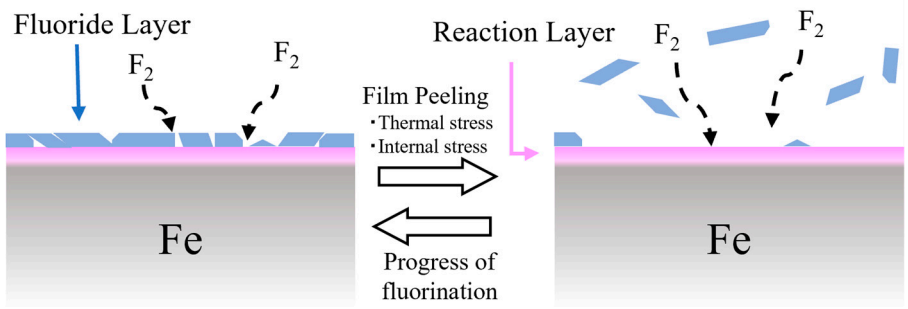

Figure 11. Peeling off the fluoride layer and progression of fluorination.

4.2. Relationship between Liquid Na Wettability and the Surface State of the Fluorinated Layer

The reason for the change in liquid Na wettability of the iron surface due to fluorination might be the difference in the chemical bonding state of the iron fluoride formed on the specimen surface. The analysis of the Fe 2p3/2 peak of the fluorinated specimen measured by XPS (Figure 2) confirms that FeF_2 or FeF_3 bonds were formed on the fluorinated iron surface, depending on the fluorination conditions. F-380-RT, F-760-RT, and F-760-200, with strong peaks of FeF_3 bonds, had smaller sliding angles than the untreated specimen in Figure 7 and were not wettable with liquid Na. In contrast, F-380-100, F-760-100, and F-380-200, with strong peaks of FeF_2 bonds, had larger sliding angles than the untreated specimen in Figure 7 and were wettable with liquid Na. From these results, we consider that the liquid Na wettability was changed depending on the bonding state of the iron fluoride formed on the iron surface.

Figure 12 shows the relationship between the contact angle hysteresis and the sliding angle obtained from the wettability test. The contact angle hysteresis is the difference between the advancing contact angle (θ_{Adv}) and the receding contact angle (θ_{Rec})—one of the indicators of the wettability of a droplet sliding down a solid surface. The larger the contact angle hysteresis, the better the lyophilic state, and vice versa.

There is a good correlation between the contact angle hysteresis and the sliding angle. Furthermore, depending on the fluorination conditions, the liquid Na wettability on the specimen surface becomes either more wettable (upper right) or less wettable (lower left) than that of the untreated specimen. The wettability test results indicate that fluorination can control the wettability of liquid Na on the iron surface in lyophilic and lyophobic states.

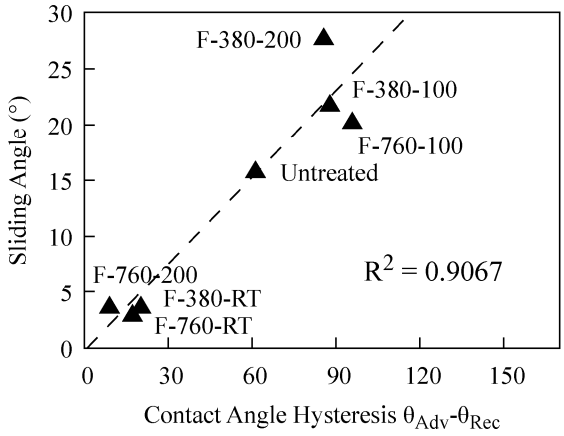

Figure 12. Relationship between the contact angle hysteresis and the sliding angle.

5. Conclusions

This study evaluated the liquid Na wettability of iron and fluorinated iron, and the following results were obtained.

(1) F-380-RT, F-760-RT, and F-760-200 specimens had large surface roughness, approximately 3–6.5 times that (27 nm) of the untreated specimen. The XPS measurement results show that a thick layer of reaction products, primarily comprising FeF_3 bonds, can be formed on the surfaces of these specimens.
(2) F-380-RT, F-760-RT, and F-760-200 specimens had small sliding angles of Na droplets at measurement and a small deformation in the Na droplet shape.
(3) The surface roughness of F-380-100, F-760-100, and F-380-200 specimens was similar to those of the untreated specimen. The XPS measurement results indicate that the surfaces of these specimens contain a large amount of FeF_2 bonds. Together with the detection of metallic iron peaks due to the etching of the outermost surface layer, a thin reaction layer primarily comprising FeF_2 bonds can be formed on their surfaces.
(4) F-380-100, F-760-100, and F-380-200 specimens had large sliding angles of Na droplets at measurement and a large deformation in the Na droplet shape.
(5) Fluorination changed the wettability between the specimen and the liquid Na to lyophilic and lyophobic states. We considered that the bond formed on the specimen surface determines whether it is easier or harder to be wetted with liquid Na.

The above results indicate that fluorination is a surface modification technique that can control the liquid Na wettability of iron.

Author Contributions: M.N.: Conceptualization, formal analysis, investigation, methodology, project administration, validation, visualization, writing—original draft. J.-i.S.: conceptualization, formal analysis, investigation, methodology, project administration, resources, supervision, validation, writing—review and editing. A.I.: investigation, validation. R.O.: investigation, validation. J.-H.K.: conceptualization, investigation, methodology, resources, validation, writing—review and editing. All authors have read and agreed to the published version of the manuscript.

Funding: This research received no external funding.

Institutional Review Board Statement: Not applicable.

Informed Consent Statement: Not applicable.

Data Availability Statement: The data related to this study are all presented in the article.

Conflicts of Interest: The authors declare no conflicts of interest.

References

1. Foust, O.J. *Sodium-NaK Engineering Handbook. Volume 1, Sodium Chemistry and Physical Properties*; Gordon and Breach Science Publishers: New York, NY, USA, 1972.

2. Chander, S.; Meikandamurthy, C.; Kalc, R.D. Experimental study of self-welding of materials in high temperature liquid sodium. *Wear* **1993**, *162*, 458–465. [CrossRef]
3. Dobosz, A.; Plevachuk, Y.; Sklyarchuk, V.; Sokoliuk, B.; Gancarz, T. Potential cooling agents for fast nuclear reactors: Sodium influence on the thermophysical properties of liquid Ga-Sn-Zn eutectic alloys. *J. Mol. Liq.* **2019**, *296*, 112024. [CrossRef]
4. Hejzlar, P.; Todreas, N.E.; Shwageraus, E.; Nikiforova, A.; Petroski, R.; Driscoll, M.J. Cross-comparison of fast reactor concepts with various coolants. *Nucl. Eng. Des.* **2009**, *239*, 2672–2691. [CrossRef]
5. Hémery, S.; Auger, T.; Courouau, J.L.; Balbaud-Célérier, F. Liquid metal embrittlement of an austenitic stainless steel in liquid sodium. *Corr. Sci.* **2014**, *83*, 1–5. [CrossRef]
6. Hémery, S.; Auger, T.; Courouau, J.L.; Balbaud-Célérier, F. Effect of oxygen on liquid sodium embrittlement of T91 martensitic steel. *Corr. Sci.* **2013**, *76*, 441–452. [CrossRef]
7. Ji, Y.; Wu, M.; Feng, Y.; Liu, H.; Yang, X.; Li, Y.; Chang, C. Experimental study on the effects of sodium and potassium proportions on the heat transfer performance of liquid metal high-temperature oscillating heat pipes. *Int. J. Heat Mass Transf.* **2022**, *194*, 123116. [CrossRef]
8. Kawaguchi, M.; Tagawa, A.; Miyahara, S. Reactive Wetting of Metallic Plated Steels by Liquid Sodium. *J. Nucl. Sci. Technol.* **2011**, *48*, 499–503. [CrossRef]
9. Griffin, J.W.; Peters, T.J.; Posakony, G.J.; Chien, H.-T.; Bond, L.J.; Denslow, K.M.; Sheen, S.-H.; Raptis, P. *Under-Sodium Viewing: A Review of Ultrasonic Imaging Technology for Liquid Metal Fast Reactors*; Pacific Northwest National Lab. (PNNL): Richland, WA, USA, 2009. [CrossRef]
10. Kim, H.W.; Joo, Y.S.; Park, C.G.; Kim, J.B.; Bae, J.H. Ultrasonic Imaging in Hot Liquid Sodium Using a Plate-Type Ultrasonic Waveguide Sensor. *J. Nondestruct. Eval.* **2014**, *33*, 676–683. [CrossRef]
11. Aizawa, K.; Sasaki, K.; Chikazawa, Y.; Fukuie, M.; Jinbo, N. Demonstration of Under Sodium Viewer in Monju. *Nucl. Technol.* **2018**, *204*, 74–82. [CrossRef]
12. Bader, M.; Busse, C.A. Wetting by sodium at high temperatures in pure vapour atmosphere. *J. Nucl. Mater.* **1977**, *67*, 295–300. [CrossRef]
13. Liang, N.; Fu, X.; Zhang, J.; Ruan, Z.; Qin, B.; Ma, T.; Long, B. Evaluation of Wetting Behaviors of Liquid Sodium on Transition Metals: An Experimental and Molecular Dynamics Simulation Study. *Materials* **2024**, *17*, 691. [CrossRef]
14. Saito, J.; Kobayashi, Y.; Shibutani, H. Wettability of Pure Metals with Liquid Sodium and Liquid Tin. *Mater. Trans.* **2021**, *62*, 1524–1532. [CrossRef]
15. Saito, J.; Monbernier, M. Relationship between the contact angle of pure Cu and its alloys owing to liquid Na and electronic states at the interface. *Surf. Interfaces* **2023**, *41*, 103248. [CrossRef]
16. Pauling, L. The nature of the chemical bond. Application of results obtained from the quantum mechanics and from a theory of paramagnetic susceptibility to the structure of molecules. *J. Am. Chem. Soc.* **1931**, *53*, 1367–1400. [CrossRef]
17. The 155 Committee of Fluorine Chemistry. *"Fusso Kagaku Nyumon" (Introduction to Fluorochemistry)*; Sankyoshuppan: Tokyo, Japan, 2004.
18. Tressaud, A.; Durand, E.; Labrugère, C. Surface modification of several carbon-based materials: Comparison between CF_4 rf plasma and direct F_2-gas fluorination routes. *J. Fluor. Chem.* **2004**, *125*, 1639–1648. [CrossRef]
19. Kim, J.H.; Mishina, T.; Namie, M.; Nishimura, F.; Yonezawa, S. Effects of surface fluorination on the dyeing of polycarbonate (PC) resin. *J. Coat. Technol. Res.* **2021**, *19*, 617–624. [CrossRef]
20. Miki, N.; Maeno, M.; Maruhashi, K.; Nakagawa, Y.; Ohmi, T. Fluorine passivation of stainless steel. *Corros. Sci.* **1990**, *31*, 69–74. [CrossRef]
21. Kobayashi, M.; Nishimura, F.; Kim, J.H.; Yonezawa, S. Dyeable hydrophilic surface modification for PTFE substrates by surface fluorination. *Membranes* **2023**, *13*, 57. [CrossRef]
22. Namie, M.; Kim, J.H.; Yonezawa, S.; Saito, J. Wettability control of stainless steel surfaces to liquid sodium by surface fluorination treatment. In Proceedings of the 45th Fluorine Conference of Japan, Kyoto, Japan, 1–2 November 2022.
23. Pouzet, M.; Dubois, M.; Charlet, K.; Béakou, A. From hydrophilic to hydrophobic wood using direct fluorination: A localized treatment. *C. R. Chim.* **2018**, *21*, 800–807. [CrossRef]
24. Namie, M.; Saito, J. Atomic interactions at the interface between iron or iron fluoride, and sodium by the first-principles calculation. *Comput. Mater. Sci.* **2024**, *239*, 112963. [CrossRef]
25. Kim, J.H.; Umeda, H.; Ohe, M.; Yonezawa, S.; Takashima, M. Preparation of pure $LiPF_6$ using fluorine gas at room temperature. *Chem. Lett.* **2011**, *40*, 360–361. [CrossRef]
26. Kasrai, M.; Urch, D.S. Electronic Structure of Iron (II) and (III) Fluorides using X-ray Emission and X-ray Photoelectron Spectroscopies. *J. Chem. Soc. Faraday Trans.* **1979**, *75*, 1522–1531. [CrossRef]